Coastal extreme sea levels in the Caribbean Sea induced by tropical cyclones

Ariadna Martín[1], Angel Amores[1], Alejandro Orfila[1], Tim Toomey[1], and Marta Marcos[1,2]

[1]Mediterranean Institute for Advanced Studies (UIB-CSIC), Spain
[2]Department of Physics, University of Balearic Islands, Spain

Correspondence: Marta Marcos (marta.marcos@uib.es)

Abstract. Every year the Caribbean Sea faces the passage of several tropical cyclones that generate coastal extreme sea levels with potential strong and hazardous impacts. In this work we simulate the storm surges and wind-waves induced by a set of 1000 tropical cyclones over the Caribbean Sea that are representative of the present-day climate. These events have been extracted from a global database of synthetic hurricanes spanning a 10,000-year period. The atmospheric forcing fields, associated to the set of tropical cyclones, are used to feed a coupled hydrodynamic-wave model with high resolution (∼2 km) along the continental and islands coasts. Given the large number of events modeled, our results allow detailed statistical analyses of the magnitude and mechanisms of coastal extreme sea levels as well as the identification of most exposed areas to both storm surges and extreme wind-waves.

1 Introduction

Tropical cyclones (TCs) are among the most hazardous natural disasters, significantly affecting population safety, economies and ecosystems in coastal areas. The Eastern coast of Central and North America are among the most affected regions to these events worldwide (Needham et al., 2015). Here we focus in the coastal regions of the Caribbean Sea, an area far less investigated when compared to the Gulf of Mexico, in spite of its exposure to TC being similar. With a relatively small landmass and total population (∼ 44 million people based on the latest United Nations estimates (woldometers, 2022)), the Caribbean has experienced, in the past two decades, 163 storm events (hurricanes and storm surges) affecting a total of 25.8 million people and resulting in over 5000 deaths (Centre for Research on the Epidemiology of Disasters, 2020). Moreover, the Caribbean Sea contains more than 700 islands. The characteristics of these tropical islands (i.e their size, coastal population density, morphology, elevation and coastal defences) make them particularly vulnerable territories to the impact of low-frequency and high-intensity events, such as TCs (Pillet et al., 2019b; Duvat et al., 2017; Giuliani and Peduzzi, 2011). Even for some of these small islands nation, the damages caused by TCs can exceed the size of their economies. This is the case of Dominica, that in 2017 was affected by Hurricane Maria causing a damage cost estimated of 226% of its 2016 gross domestic product (GDP) (GFDRR, 2017). Another example is Grenada, affected by Hurricane Ivan in 2004 that caused an economic damage exceeding 200% of their GPD (ECLAC, 2004). As the socio-economy of small islands depends on the preservation of the coastal zone, it is crucial to investigate and support hurricane risk mitigation efforts in these areas.

25   TCs are a relatively rare phenomenon with around 90 (± 10) formations per year globally. In addition, historical records of TCs are in general scarce, since reliable TC dataset are only available from 1980 onwards (Bloemendaal et al., 2020). In consequence, there have been earlier studies that are limited to particular small areas, islands or bays, where observations are available during the passage of a TC. This is the case for example of Batabanó, Samaná Bay, Guadeloupe and Dominica (Arenal et al., 1998; Krien et al., 2015). One way to overcome the historical lack of observations of TCs is the generation

30   of synthetic hurricane databases, built consistently with the observed TCs characteristics that allow more robust statistical analyses of TCs frequency and intensities and that can be used to evaluate the associated risks (Appendini et al., 2017; Lin et al., 2014). This study will take advantage of one of these synthetic hurricane databases by Bloemendaal et al. (2020) that is used here to provide an unified Caribbean-wide view of the marine hazards generated by TCs. In particular, we focus on the ocean hazards generated by TCs in terms of wind-waves and storm surges, using a set of 1000 hurricanes extracted from the

35   synthetic dataset combined with a fully coupled hydrodynamic-wave model. We analyse in detail the outputs of the numerical simulations to quantify the role of the different forcing factors to coastal extreme sea levels from TCs, namely, the atmospheric pressure, the wind and the wind-waves.

This paper is structured as follows: in section 2 we describe the different datasets used together with the numerical model. Section 3 include the results of wind-waves and sea surface elevation along the Caribbean coastlines. Summary and conclusions

40   are given in Section 4.

2   Data and Methods

2.1   Data

The tracks of synthetic hurricanes were extracted from STORM (Synthetic Tropical cyclOne geneRation Model) dataset (Bloemendaal et al., 2020). It consists of 10000 years of TCs over the globe obtained using a fully statistical model approach fed

45   with observed TC tracks and, thus, being representative of present-day climate conditions. This dataset provides, for each TC, its track, minimum pressure, maximum wind speed, and the radius of maximum speed with a 3-hourly time step during its lifetime. Within the 10000-year synthetic TC available in the STORM dataset, 25494 of them affected the Caribbean Sea ($\sim 2.5\,\mathrm{TC/year}$). This rate is in agreement with the 2.7 TC per year observed from 1944 to 1970 (Goldenberg et al., 2001) and the 2.47 TC per year published in Chenoweth (2006) computed from 155 years of records. Among the entire set of TC

50   affecting the Caribbean, we aim at selecting a subsample in such a way that it is statistically consistent with the original sample in terms of the TC intensity and its spatial distribution (Fig. 1) and, at the same time, small enough as to perform basin-wide numerical simulations. Following Toomey et al. (2022), to choose the size of the subsample, we compared the probability distribution functions (PDF) of the original dataset (corresponding to the 25494 TCs), and the selected samples (with sizes ranging between 10 to 10000 events) on the basis of two statistical tests, namely the root-mean-square-deviation (RMSD, Fig.

55   1a) and the correlation (Fig. 1b). This process was performed 1000 times for each size of the subsamples (selecting randomly the events each time) and for both the maximum speed and the spatial distribution of the TCs tracks PDFs. In this case the PDF is built using the number of hurricanes passing trough each pixel of the grid (the spatial domain has been divided into 2 degrees

bins, represented in Fig. 1, while for the maximum speed distribution the bins size was fixed at 2m/s. We seek to determine a size for the subsample that is a good representation of the original distribution and also small enough as to perform the

60 numerical simulations described in section 2.3 within a reasonable computational time. Our results (Fig. 1a and c) indicate that a subsample of 1000 hurricanes is statistically consistent to the original distribution, both in intensity and spatial distribution in this area. The maps in Fig. 1 represent this behaviour, showing the percentage of hurricanes per pixel for the total sample (panel e) and the selected sub-sample (1000 hurricanes, panel f).

In addition to the synthetic hurricanes described above, two real events were studied. These correspond to Hurricane Wilma

65 (2005), which intensified from a 111 km/h tropical storm to a 278 km/h category 5 hurricane in less than 24 hours, an unprecedented event for an Atlantic TC that claimed 23 lives (Pasch et al., 2006) (track with diamonds in Fig. 2); and hurricane Tomas (2010), which entered into the Caribbean Sea crossing the island of St. Vincent and reached category 2 intensity (track with stars in Fig. 2). Tomas was responsible for a total of 44 fatalities in the Lesser and Greater Antilles and a total damage estimated as 336.15 million U.S dollars (Pasch and Kimberlain, 2011). The atmospheric fields required to simulate these

70 hurricanes, i.e. pressure relative to mean sea level and 10 m-wind speed, were extracted from ERA5 reanalysis (available at: https://cds.climate.copernicus.eu/, last access: 8 September 2020, Hersbach et al. (2020)). ERA5 is a comprehensive reanalysis, from 1979 to near real time, considered as a high-potential dataset (Tarek et al., 2020), that combines vast amounts of historical observations into global estimates using advanced modelling and data assimilation systems (Hersbach et al., 2020). This reanalysis has a 1-hour time step and spatial resolution ~ 30 km in the area of concern. The above-mentioned fields were

75 recovered between 14-28 October 2005 and between 27 October and 13 November 2010 for hurricanes Wilma and Tomas, respectively.

Coastal sea-level observations from tide gauges and wind-wave measurements from in-situ buoys have been used to validate the numerical simulation of the two real hurricanes Wilma and Tomas. Sea level data was obtained from GESLA dataset (https://gesla.org/, Woodworth et al. (2016)) which contains a total of 46 sea level records in the Caribbean Sea. Unfortunately,

80 given their location no footprint of any of these two hurricanes was measured by any of the available tide gauges, thus the validation of the sea surface elevation was not possible. The wind-wave measurements were retrieved from the National Data Buoy Center (1971) (NOAA, https://www.ncei.noaa.gov/archive/accession/NDBC-CMANWx, last access: 2 September 2020). A total of 47 buoys were available during the passage of the hurricanes, of which we have selected the two closest to their pathways (Fig. 2).

85 **2.2 Generation of 2D fields from synthetic tracks**

The 1000 synthetic TCs tracks extracted from STORM dataset were used to built the 2D atmospheric fields required to force the numerical model. Atmospheric pressure and surface wind fields were generated onto a 5-km regular grid using the same temporal resolution of the synthetic tracks (3 hours). The wind field accounts for a translational component that drives the hurricane forward and a dominant circular component. The former was calculated using the track, while the radial component

90 was calculated based on the empirical Holland wind profile (Holland, 1980) with the latest revision of the formulation (Holland et al., 2010). This formulation has been extensively used for reconstructing hurricane wind fields (Sitkowski et al., 2011; Boose,

2004). Translational and circular wind velocity components were added, after setting the translational component to zero at distances greater than 300 km from the hurricane eye. The final step for the wind fields consists of reducing the velocity by 20 % over land areas.

95 ## 2.3 Numerical model

We simulated storm surges and wind-waves caused by the 2D fields derived from the synthetic and the two real TCs over the Caribbean Sea using the last version of SCHISM model (Semi-implicit Cross-scale Hydroscience Integrated System Model, Zhang et al. (2016)), a state-of-art cross-scale hydrodynamic model, which is a derivative product built from the original SELFE (Zhang and Baptista, 2008). Here we have used the hydrodynamic core in its depth-average (2DH) barotropic mode
100 fully coupled with the spectral wave model WWM-III (Roland et al., 2012).

The bathymetry used for the hydrodynamic model and the spectral wave model was GEBCO 2020 (available at: https://www.gebco.net/data_and_products/gridded_bathymetry_data, (GEBCO, 2020)) on a 15 arc-second geographic latitude and longitude grid, which in the Caribbean Sea region corresponds to ~ 450 m. Both models were implemented using the same unstructured grid (generated using the Triangle algorithm (Shewchuk, 1996)) that covers the whole Caribbean Sea and part of
105 the Atlantic Ocean with a total of 135759 nodes (Fig. 2). The spatial resolution varies as a function of the depth, within a range of around 40 km in open ocean down to ~ 2 km along the coastlines. The coastline used was downloaded from https://osmdata.openstreetmap.de/data/coastlines.html which, on average, has a spatial resolution of approximately 40 m (OpenStreetMap contributors, 2017). The resolution of the coastline was reduced to 2 km, except in areas with abrupt changes in the coastline.

The computational domain (Fig. 2) was chosen to include the prevailing TC incoming directions. Although hurricanes
110 affecting the Caribbean Sea can develop further inside the Atlantic Ocean, from the coast of West Africa, the selected domain is large enough to allow a correct generation and propagation of the wind-waves originated by hurricanes affecting the Antilles (i.e. it accommodates enough space for the wind fetch to act). There are two open boundaries in the model, both with free elevation and velocity forced to 0, corresponding to the Atlantic ocean boundary and the region between Cuba and Mexico (black lines Fig. 2).

115 The spectral domain for the wind wave model has been fixed to 24 bins for both direction (i.e., 15° bins) and frequency (ranging between 0.04 to 0.6 Hz). For the bottom friction the Manning's drag coefficient was fixed to 0.02 and the wind stress was calculated using Pond & Pickard formulation (Pond and Pickard, 1983). The computational time step was set to 10 minutes for the hydrodynamical model and 30 minutes for the wave model. The selected variables (significant wave height, sea surface elevation, air pressure, wind speed, wave peak period, and wave peak direction) were saved every hour. The model
120 configuration was defined after model validation for the two real events, with a reasonable computational cost (see Sec. 3.2).

In order to analyse the role of the different contributions of the atmospheric forcing fields, i.e. atmospheric pressure, wind and the wind-waves, four different numerical simulations where performed for each hurricane: (1) a fully coupled run between the hydrodynamic model and the wind-wave module that takes into account all contributions as well as their coupling; (2) a run using only the hydrodynamic model forced with atmospheric pressure and wind; here the contribution of the wind-waves
125 is excluded; (3) a hydrodynamic model run forced using only the atmospheric pressure, the winds were fixed to 0 m/s; and

(4) a hydrodynamic model run forced only by the wind, setting the atmospheric pressure constant to 101325 Pa. Finally, the contribution of the wind-waves was extracted from the differences between runs number 1 and 2 which accounts for all the couplings, while the effects of the atmospheric pressure and wind could directly be quantified from the simulations 3 and 4, respectively. The method for obtaining the pure contribution of each factor, as well as the synergistic effect due to the mutual

130 interactions among two or more of these factors should be carried out using 2^n simulations, where n is the number of forcings to be separated. Thus, the wind and pressure contributions were correctly separated, while the wind-waves contribution implicitly includes all the couplings with the other forcing interactions (wind-waves - wind, wind-waves - pressure and the wind-waves - pressure - wind term), of which we assume are small compared to the main contribution of wind-waves (Amores et al., 2020).

The computational time of each hurricane was $\sim$ 3 hours for the fully coupled runs using only one CPU. In our case, we

135 used 20 processors which allowed us to reduce the computational time to approximately 10 days by running simultaneously 20 hurricanes. For the hydrodynamic runs in which the wind-wave model is not used, the total computational time was about two days per configuration (including the 1000 TC). This leads to a total computational time of approximately 2 weeks.

3 Results

3.1 Characteristics of TC affecting the Caribbean Sea.

140 The characteristics of the TCs affecting the Caribbean coastlines are represented in Fig. 3 in terms of their frequency and intensity. The frequency of TCs along the coasts presents a well defined geographic pattern (Fig. 3a): while the eastern part of the basin receives over 3 TCs per decade, the western coasts are affected on average by less than 1 per decade. The southern coast of the Caribbean (north of South America) barely sees any TC because of their prevailing travelling direction towards the west-northwest which suggests that the energy is dissipated before reaching those coasts. The areas affected by a larger number

145 of TCs include the West Indies, the islands of La Española (Dominican Republic and Haiti) and Puerto Rico, which are heavily exposed to Atlantic hurricanes. Given the clear spatial differences, it is important to distinguish two different families of TCs, that can be classified depending on their region of origin, either in the Atlantic Ocean or inside the Caribbean Sea. Each one of these families has a distinct footprint along the Caribbean coastlines, with the eastern part of the Caribbean Sea being affected only by hurricanes generated in the Atlantic Ocean and the western coasts being hit by both families although primarily by those

150 originated within the same basin. This pattern is displayed in Fig. 3c and d where the median intensities of the two families of TCs affecting each coastal point are represented. The TCs from Atlantic Ocean (panel d) are the more intense reaching maximum speeds exceeding 200 km/h, while these values are around 125 km/h for TC generated within the Caribbean (note the different colour scales in the maps). Interestingly, the most intense TCs hit the western part of the Caribbean coastlines; the reason is that these hurricanes, that are strong in origin, are further intensified during their trip through the warm Caribbean

155 Sea. Regarding the areas exposed to both families of TCs, the western part of Cuba is the area hit by the most intense TCs. Although the hurricanes affecting the lesser Antilles are not the most intense ones, the greater number of them makes this area one of the most exposed to their impacts.

These results have been obtained using the TCs from the selected subset. When the same maps are produced with the complete TC dataset, the patterns are essentially identical with the only exception in the number of Caribbean TCs and their

160   intensities affecting the Antilles (see Fig. S1c). The difference comes from a few hurricanes in the complete dataset that are generated into the Caribbean Sea and move eastwards, instead of westwards predominant direction. This is an extremely rare phenomenon, accounting for less than 20 TCs from the 25494 available in the dataset, that represents less than 0.001% of the total number of TCs generated in the Caribbean Sea. Thus it is not surprising that they are not represented in the subset.

3.2   Model Validation.

165   The numerical simulations of hurricane Wilma and Thomas described in section 2.1 (see their tracks in Fig. 2) were used to validate the model configuration against ocean observations. To do so, significant wave height (H_s) from buoy measurements (diamonds for hurricane Wilma and star for hurricane Thomas in Fig. 2) were compared with the modelled time series of the closest grid point (Fig. 4) during each event. In general there is a very good agreement between observed and modelled H_s. In the case of hurricane Wilma, correlation is above 0.90 for all buoys and the maximum RMSD is 0.68 m; for hurricane Thomas

170   the agreement is even better (correlations above 0.94) and only 0.3 m of maximum RMSD. Model validation for the sea surface elevation (SSE) was not possible since there have not been TCs that passed closed enough to a tide gauge location as to leave a footprint in the SSE record (Torres and Tsimplis, 2014). The same applies to radar altimetry data that measure sea level, and provides Sea Level Anomaly, however, no records have been found for these hurricanes.

3.3   Coastal wind-waves induced by TCs.

175   The metric chosen to characterise the wave hazards induced by TCs along the coastlines has been defined as the 99th percentile of the set of maximum H_s for each hurricane at every coastal grid point (i.e., a measure of the ten most intense hurricanes from the 1000 simulated for each particular location). The results are mapped in Fig. 5, which includes an inset with a zoom in the Lesser Antilles. The highest values, exceeding 10 m and reaching almost 20 m in some areas, are found in the West Indies, including the islands of La Española (Dominican Republic and Haiti) and Puerto Rico, and in the Caribbean coast of Mexico. It

180   is worth noting that the highest waves hitting the Lesser Antilles (Fig. 5b) are found in their eastern coasts, as expected as they are mainly hit by TCs of Atlantic origin travelling westwards. The Atlantic hurricanes, that are generally more intense than those generated in the Caribbean Sea (Fig. 3c and d), originate high waves in the central Atlantic basin that have a long fetch before reaching the Antilles. These islands act as a barrier and prevent the large waves from entering the Caribbean Sea. After crossing the Antilles, these hurricanes continue travelling inside the Caribbean Sea, but the generated waves are less intense

185   due to the smaller fetch area.

The peak direction (D_p) of wave propagation along the Caribbean coastlines is perpendicular to the coast due to wave refraction, regardless the hurricane family (Fig. 5c). The main peak period (T_p) found in the Caribbean region for hurricane-generated ocean waves (Fig. 5d) has values between 14 and 18 s. Smaller periods (around 6 s) are observed in areas with the greatest influence of hurricanes originating inside the Caribbean Sea (Fig. 3.1b) or in particularly protected areas such as the

190   southern coast of Cuba or the coast of Belize, or in the enclosed bay of Haiti where its capital city, Puerto Principe, is located.

Other protected areas with low T_p include Maracaibo lake in Venezuela and the Gulf of Paria in Trinidad and Tobago island, although here H_s is negligible.

3.4 Sea surface elevation induced by TCs.

Following the same metric used for waves, the 99th percentile of the set of the maximum SSE for each hurricane at every
195 coastal point has been used to describe the spatial distribution of extreme SSE generated by TCs (Fig. 6). Here we focus on total SSE changes and its counterparts caused by the atmospheric pressure, by winds and by wave-setup, which is the elevation of the sea surface due to breaking waves (Gregory et al., 2019). To do that, four different numerical simulations were performed for each hurricane as explained in section 2.3.

The largest values of coastal SSE ($> 2m$) (Fig. 6a) are found along the coastlines of Cuba and Belize, where the H_s is lower
200 (Fig. 5a), because of their shallow coastal waters that favour the wind setup. SSE values as low as 20 cm are obtained along the southern coasts of the basin, far from the main pathway of TCs (Fig. 3a). Regarding the role of each component to the total SSE, the wave-setup is negligible almost everywhere (Fig. 6a). Its contribution reaches a maximum of around 25 cm in the shallow areas of Belize, Mexico and the southern coast of Cuba mentioned before and it represents less than 5% of the total contribution (see Fig.S2b). The reason is that the wave-setup is very likely underestimated due to the relatively coarse coastal
205 resolution of the model grid that is not able to represent properly the shallow water wave dynamics. Wind-setup (Fig. 6c) is the most important contribution, specially in the western Caribbean coastlines where it can reach up to 2 m. The eastern coasts are dominated by the effects of the low atmospheric pressure associated to TCs (Fig. 6d, note the different colour-scales), with a contribution of around 0.5 m in this area. It is evident that there must be a relationship between the distance to the eye of the TC and the increase in SSE in response to atmospheric pressure changes (Fig. S3). If, for each coastal point, the number
210 of hurricanes at a distance less than twice the radius of maximum speed are selected, a very similar pattern to the atmospheric pressure contribution to the total SSE emerges (Fig. 3d). Summarizing, in terms of SSE induced by TCs, the eastern Caribbean coastlines are mainly affected by the atmospheric pressure contribution, while the main driver in the western area is the wind setup. These geographic patterns are the result of the combination of two different mechanisms: 1) the crossing of TCs of Atlantic origin over the eastern coasts leaving their footprint in atmospheric pressure and 2) the shallow continental shelf
215 along the western coasts, that allows the water to accumulate due to the effect of the wind. The effects of wave setup are not accounted for due to the spatial resolution, so the numbers of SSE represent a lower bound of hurricane-induced coastal sea level extremes.

3.5 Computation of return levels of coastal waves and sea surface elevation

Return levels for extreme coastal waves and SSE at every coastal grid point have been calculated using a Generalized Pareto
220 Distribution (GPD) to all measurements over a chosen threshold. Using POT (Peaks Over Threshold) analysis together with GPD, increases the number of measurements included in the analysis, and correspondingly reduces the statistical uncertainty of quantile variances (Brabson and Palutikof, 2000). Studying return periods for events such as hurricanes adds a difficulty in selecting the threshold, since by definition they are all extremes. However, each event affects different areas of the Caribbean

Sea, so that is not appropriate to set a common threshold for the entire area of study; rather, the threshold has been chosen for
225 every grid point. For this purpose, the data at each grid point have been adjusted to a GPD successively, each time removing
one value from the adjustment. The threshold is considered as the point where the GPD stabilises and all the return levels
remain constant regardless the value of threshold, we consider this point as the threshold of the extremes of each area (for
periods ranging between 1 and 500 years, specifically for 10,50,100,200 and 500 years).

The return levels associated to the 100-year return period of H_s and SSE generated by TCs are shown in Fig. 7a and b,
230 respectively. The spatial distribution of the return levels for the H_s (Fig. 7a) and SSE (Fig. 7b) mimic the geographic patterns
in Fig. 5a and Fig. 6a, respectively, as expected. The 100-yr return periods of H_s exceed 12 m in West Indies and most of the
northern coasts, including Puerto Rico, Dominican Republic and the eastern part of Cuba. Cuba is also affected by the largest
SSE (panel b) reaching up to 2 m. High return levels of SSE are also observed in the coast of Mexico, Belize and a small part
of Guatemala. Finally, the southern Caribbean coast, once again, has the lowest values of both H_s and SSE return levels, being
235 in some places even null, such as the coasts of Panama. These are, therefore, the safer coastlines in the Caribbean Sea in terms
of coastal hazards, as far as TCs are concerned.

4   Summary and Discussion

In this study we have analysed, for the first time, the coastal extreme sea levels generated by present-day tropical cyclones
in the Caribbean Sea by numerically simulating the sea level elevations and the wind waves from a 1000 synthetic tracks
240 selected from STORM dataset. Two well-differentiated families of TCs have been identified depending on their generation
region (Fig. 3): the Atlantic basin family, formed by very powerful hurricanes that mainly affect the coasts of the Antilles,
Puerto Rico, La Española and Cuba; and the Caribbean basin family which generates off the coast of Honduras and mainly
affects the eastern coasts of the Caribbean Sea. The main differences between both families, besides their generation area, are
1) the length of their tracks, having the Atlantic TCs longer life-times travelling longer distances before their first landfall;
245 and 2) their intensity (maximum wind speed), being the Atlantic TCs much more intense than the Caribbean TCs due to their
longer life-times travelling over a warm sea. The projected changes in the large-scale steering flow from increasing greenhouse
gases are expected to change their genesis location and shift their tracks (Colbert et al., 2013). These changes would affect both
families differently, declining the frequency of Caribbean hurricanes and increasing those of the Atlantic basin. For the latter,
an eastward shift on their tracks is also expected, what would translate into a decrease in the number of Atlantic TCs affecting
250 the Caribbean coasts.

The Atlantic-facing eastern coast of the Caribbean basin is the one affected by the largest waves generated by TCs (Fig.
5), easily exceeding 10 m of H_s and being especially large in the Lesser Antilles (Barbados, Saint Lucia, Martinique and
Dominica), where H_s can reach 16 m, corresponding to a 50-years return period. These results are consistent with the historical
records of major TCs impacting these islands. Hurricane Hugo, that hit Guadalupe and Puerto Rico in 1989, caused severe
255 damages in low-lying coastal areas, both in fatalities (56 people) and properties ($17.4 billion) (Krien et al., 2015). A more
recent example is hurricane Maria in 2017, a 5-category tropical cyclone that caused almost 200 deaths (Pasch et al., 2018),

although later counts reached 3000 fatalities[1]; and Hurricane Irma, that affected the same area two weeks later (Cangialosi
et al., 2018), proving that the West Indies are an oversea region that lies within the tracks of powerful hurricanes originating
in the Atlantic basin. In the northern area, the coasts of the Dominican Republic stand out as another hot spot of large wind
260   waves induced by TCs, specially in its southern side near the capital, Santo Domingo, with H_s exceeding 14 m. This is one
of the most heavily populated and densely built-up areas of the island and, consequently, most exposed to hurricane-induced
hazards. This was evidenced by Hurricane David, a category 5 TC that hit this island in 1979 which was responsible for 2068
deaths, 2000 of which occurring in its capital (Hebert, 1980).

        Other studies limited to some sectors of the Caribbean coastlines have identified regions as the most affected by the wind-
265   waves generated by TCs. For example, (Pillet et al., 2019a) identified as one of the most vulnerable areas the east coast of the
West Indies, affected by H_s larger than 15 m, and (Montoya et al., 2018) pointed to the northern area of the Caribbean sea, near
Jamaica, Puerto Rico, Dominican Republic and Haiti, as the regions inside the Caribbean Sea with largest 30-year return-level
H_s. These are in agreement with our findings. Ignoring possible changes in the tracks of hurricanes affecting the Caribbean
basin (Colbert et al., 2013), changes in H_s from TC intensification due to rising sea surface temperatures (SST) are expected
270   to be minor, with the largest increase not exceeding 25 cm in the Colombin Basin (Kleptsova et al., 2021). As a result patterns
of H_s would remain similar to those seen in Fig. 5 and 7. However, this is not the case if the effects of the projected increase
in intensity of such hurricanes are considered (Murakami et al., 2014), as these could result in higher return levels than those
calculated.

        The largest sea surface elevations generated by TCs were found along the northwestern area of the Caribbean Sea (Cuba,
275   Mexico and Belize) in agreement with Torres and Tsimplis (2014), despite this are not directly affected by the most intense
hurricanes. SSE is very dependent on the morphology of the coastlines, which in this case is formed by very narrow and shallow
bays located behind cays that allow the generation of storm surges larger than 2 m, provided that the shelf is well represented in
the model bathymetry. Indeed, the largest storm surges registered in the Caribbean Sea are in the Gulf of Batabanó (Cuba) with
a value of more than 2 m (Arenal et al., 1998, 2016). On the contrary, the TC-induced SSE in the Antilles, the area affected by
280   the most intense hurricanes, is not among the largest simulated ($< 0.5\,m$). In this case, the lack of a continental shelf or narrow
and shallow bays behind cays in front of the coastlines do not allow the accumulation of water having as a result smaller SSEs
than other regions affected by less intense hurricanes. Another SSE hot spot is located in the northern coast of Nicaragua with
values exceeding 0.8 m. This section of coastline, that is mainly affected by the less intense Caribbean hurricanes, has a wide
and shallow continental shelf, prone to the development of storm surges. The smaller SSE values were found in the southern
285   coastlines of the Caribbean basin because this region is not affected by TCs at all (Fig. 3.1). It is worth noticing that the SSE
in the Yucatan Channel, between Mexico and Cuba, may be overestimated because it is part of one of the boundaries of the
model. In fact, all these zones are flooding hot areas where, in concordance with Dullaart et al. (2021), the number of people
exposed to a flood event relative to to the global population due to TCs storm surges contribution is especially large ($> 90\%$),
both in Cuba and Belize.

---

[1]https://www.nytimes.com/2018/08/28/us/puerto-rico-hurricane-maria-deaths.html

290   We have also investigated the contribution of each mechanism (atmospheric pressure, wind setup and wave setup) to the total
SSE which strongly varies between different regions of the Caribbean Sea. The largest contribution of the atmospheric pressure
is found in areas located along the hurricane tracks. The wind contribution is strongly related to the morphology of the coast
and with continental shelves. Wave setup contributions are also located in shallow areas that allow the accumulation of water.
However, this contribution is underestimated due to the relatively coarse resolution of the model grid that prevents reproducing
295   properly the waves transformation in shallow waters. Mean sea-level rise will increase the water depths and is likely to cause
a decrease in the contribution of wind setup and wave setup (Kleptsova et al., 2021) while keeping the atmospheric pressure
contribution equal.

This study provides a regional overview of the coastal hazards induced by TC in the Caribbean Sea. The model simulations
provide a complete mapping of the extreme wind-waves and storm surges along the coasts and identifies the dominant mecha-
300   nisms as well as the type of TC (in terms of their origin) and the areas that are most affected by each of them along with return
levels for 10, 20, 50, 100, 200, 500-years return periods. Limitations of our study include: 1) the fact that our forcing fields
have been generated using synthetic tracks and using parameterised pressure and wind profiles possibly leading to inaccurate
2D fields; 2) low bathymetry resolution which causes 3) underestimated wave setup; and 4) a possible SSE overestimation may
be taking place in the Yucatán Channel since is part of one of the open boundaries of the model.

305   *Data availability.*   The return levels of H_s and SSE corresponding to 10, 50, 100, 200 and 500 years along all coastal grid points are available
at the data repository 10.5281/zenodo.6417429

Author contributions.   AA and MM conceived the work and designed the numerical experiments. AM retrieved the atmospheric forcings and
performed the numerical simulations. AA, AM and MM analysed the outputs and all the authors contributed to the outline and writing of the
manuscript.

310   *Competing interests.*   The authors declare that they have no conflict of interest.

Acknowledgements.   Grant RTI2018-093941-B-C31 funded by MCIN/AEI/ 10.13039/501100011033 and by "ERDF A way of making Eu-
rope".

References

Amores, A., Marcos, M., Carrió, D. S., and Gómez-Pujol, L.: Coastal impacts of Storm Gloria (January 2020) over the north-western Mediterranean, Natural Hazards and Earth System Sciences, 20, 1955–1968, https://doi.org/10.5194/nhess-20-1955-2020, 2020.

Appendini, C. M., Pedrozo-Acuña, A., Meza-Padilla, R., Torres-Freyermuth, A., Cerezo-Mota, R., López-González, J., and Ruiz-Salcines, P.: On the role of climate change on wind waves generated by tropical cyclones in the Gulf of Mexico, Coastal Engineering Journal, 59, 1740 001, 2017.

Arenal, I. M., Parrado, R. P., García, I. S., Concepción, O. G., Pérez, M. B., Allen, Y. J., Padrón, P. B., and Pérez, A. L.: " THE COASTAL FLOODS IN THE CUBAN TERRITORY, THE MOST SENSITIVE AREAS AND THE POSSIBLE IMPACT OF THE CLIMATE CHANGE, Institute of Meteorology, 23, 50–62, 1998.

Arenal, I. M., Baños, I. H., Valdés, E. G., Mayo, A. H., Rodríguez, O. O. D., Llamo, A. V., and Zas, J. A. R.: The Coastal Flood Regime around Cuba, the Thermohaline Structure Influence and Its Climate Tendencies, 2016.

Bloemendaal, N., Haigh, I. D., de Moel, H., Muis, S., Haarsma, R. J., and Aerts, J. C.: Generation of a global synthetic tropical cyclone hazard dataset using STORM, Scientific data, 7, 1–12, 2020.

Boose, E.: A method for reconstructing historical hurricanes, Hurricanes and Typhoons: Past, Present, and Future, 99, 120, 2004.

Brabson, B. and Palutikof, J.: Tests of the generalized Pareto distribution for predicting extreme wind speeds, Journal of applied meteorology, 39, 1627–1640, 2000.

Cangialosi, J. P., Latto, A. S., and Berg, R.: Hurricane Irma (AL112017): 30 August–12 September 2017, National Hurricane Center Tropical Cyclone Report, 111, 2018.

Centre for Research on the Epidemiology of Disasters, U. N. O. f. D. R. R. U.: The Human Cost of Disasters. An Overview of the Last 20 Years (2000–2019), 2020.

Chenoweth, M.: A reassessment of historical Atlantic basin tropical cyclone activity, 1700–1855, Climatic Change, 76, 169–240, 2006.

Colbert, A. J., Soden, B. J., Vecchi, G. A., and Kirtman, B. P.: The impact of anthropogenic climate change on North Atlantic tropical cyclone tracks, Journal of climate, 26, 4088–4095, 2013.

Dullaart, J. C., Muis, S., Bloemendaal, N., Chertova, M. V., Couasnon, A., and Aerts, J. C.: Accounting for tropical cyclones more than doubles the global population exposed to low-probability coastal flooding, Communications Earth & Environment, 2, 1–11, 2021.

Duvat, V. K., Magnan, A. K., Wise, R. M., Hay, J. E., Fazey, I., Hinkel, J., Stojanovic, T., Yamano, H., and Ballu, V.: Trajectories of exposure and vulnerability of small islands to climate change, Wiley Interdisciplinary Reviews: Climate Change, 8, e478, 2017.

ECLAC: The impact of hurricane Ivan in the Cayman Islands, Economic Commission for Latin America and the Caribbean, https://www.cepal.org/en/publications/25728-impact-hurricane-ivan-cayman-islands, 2004.

GEBCO: General Bathymetric Chart of the Ocean, https://www.gebco.net/,lastaccess:9October2020, 2020.

GFDRR: Post-Disaster Needs Assessment Hurricane Maria, Global Facility for Disaster Reduction and Recovery, https://www.gfdrr.org/sites/default/files/publication/Dominica_mp_012418_web.pdf, 2017.

Giuliani, G. and Peduzzi, P.: The PREVIEW Global Risk Data Platform: a geoportal to serve and share global data on risk to natural hazards, Natural Hazards and Earth System Sciences, 11, 53–66, 2011.

Goldenberg, S. B., Landsea, C. W., Mestas-Nuñez, A. M., and Gray, W. M.: The recent increase in Atlantic hurricane activity: Causes and implications, Science, 293, 474–479, 2001.

Gregory, J. M., Griffies, S. M., Hughes, C. W., Lowe, J. A., Church, J. A., Fukimori, I., Gomez, N., Kopp, R. E., Landerer, F., Le Cozannet, G.,
350   et al.: Concepts and terminology for sea level: Mean, variability and change, both local and global, Surveys in Geophysics, 40, 1251–1289,
       2019.

Hebert, P. J.: Atlantic hurricane season of 1979, Monthly Weather Review, 108, 973–990, 1980.

Hersbach, H., Bell, B., Berrisford, P., Hirahara, S., Horányi, A., Muñoz-Sabater, J., Nicolas, J., Peubey, C., Radu, R., Schepers, D., et al.:
       The ERA5 global reanalysis, Quarterly Journal of the Royal Meteorological Society, 146, 1999–2049, 2020.

355 Holland, G. J.: An analytic model of the wind and pressure profiles in hurricanes, Monthly weather review, 108, 1212–1218, 1980.

Holland, G. J., Belanger, J. I., and Fritz, A.: A revised model for radial profiles of hurricane winds, Monthly weather review, 138, 4393–4401,
       2010.

Kleptsova, O. S., Dijkstra, H. A., van Westen, R. M., van der Boog, C. G., Katsman, C. A., James, R. K., Bouma, T. J., Klees, R., Riva, R. E.,
       Slobbe, D. C., et al.: Impacts of Tropical Cyclones on the Caribbean Under Future Climate Conditions, Journal of Geophysical Research:
360   Oceans, 126, e2020JC016 869, 2021.

Krien, Y., Dudon, B., Roger, J., and Zahibo, N.: Probabilistic hurricane-induced storm surge hazard assessment in Guadeloupe, Lesser
       Antilles, Natural Hazards and Earth System Sciences, 15, 1711–1720, 2015.

Lin, N., Lane, P., Emanuel, K. A., Sullivan, R. M., and Donnelly, J. P.: Heightened hurricane surge risk in northwest Florida revealed from
       climatological-hydrodynamic modeling and paleorecord reconstruction, Journal of Geophysical Research: Atmospheres, 119, 8606–8623,
365   2014.

Montoya, R. D., Menendez, M., and Osorio, A. F.: Exploring changes in Caribbean hurricane-induced wave heights, Ocean Engineering,
       163, 126–135, 2018.

Murakami, H., Li, T., and Hsu, P.-C.: Contributing factors to the recent high level of accumulated cyclone energy (ACE) and power dissipation
       index (PDI) in the North Atlantic, Journal of climate, 27, 3023–3034, 2014.

370 Needham, H. F., Keim, B. D., and Sathiaraj, D.: A review of tropical cyclone-generated storm surges: Global data sources, observations, and
       impacts, Reviews of Geophysics, 53, 545–591, 2015.

OpenStreetMap contributors: Planet dump retrieved from https://planet.osm.org , https://www.openstreetmap.org, 2017.

Pasch, R. J. and Kimberlain, T. B.: Tropical Cyclone Report Hurricane Tomas 29 October -7 November 2010, 2011.

Pasch, R. J., Blake, E. S., III, H. D. C., and Roberts, D. P.: Tropical Cyclone Report Hurricane Wilma 15-25 October 2005, 2006.

375 Pasch, R. J., Penny, A. B., and Berg, R.: National Hurricane center tropical cyclone report: Hurricane Maria, TROPICAL CYCLONE
       REPORT AL152017, National Oceanic And Atmospheric Administration and the National Weather Service, pp. 1–48, 2018.

Pillet, V., Duvat, V. K., Krien, Y., Cécé, R., Arnaud, G., and Pignon-Mussaud, C.: Assessing the impacts of shoreline hardening on beach
       response to hurricanes: Saint-Barthélemy, Lesser Antilles, Ocean & Coastal Management, 174, 71–91, 2019a.

Pillet, V., Duvat, V. K., Krien, Y., Cécé, R., Arnaud, G., and Pignon-Mussaud, C.: Assessing the impacts of shoreline hardening on beach
380   response to hurricanes: Saint-Barthélemy, Lesser Antilles, Ocean & Coastal Management, 174, 71–91, 2019b.

Pond, S. and Pickard, G. L.: Introductory dynamical oceanography, Gulf Professional Publishing, 1983.

Roland, A., Zhang, Y. J., Wang, H. V., Meng, Y., Teng, Y.-C., Maderich, V., Brovchenko, I., Dutour-Sikiric, M., and Zanke, U.: A fully
       coupled 3D wave-current interaction model on unstructured grids, Journal of Geophysical Research: Oceans, 117, 2012.

Shewchuk, J. R.: Triangle: Engineering a 2D quality mesh generator and Delaunay triangulator, in: Workshop on Applied Computational
385   Geometry, pp. 203–222, Springer, 1996.

Sitkowski, M., Kossin, J. P., and Rozoff, C. M.: Intensity and structure changes during hurricane eyewall replacement cycles, Monthly Weather Review, 139, 3829–3847, 2011.

Tarek, M., Brissette, F. P., and Arsenault, R.: Evaluation of the ERA5 reanalysis as a potential reference dataset for hydrological modelling over North America, Hydrology and Earth System Sciences, 24, 2527–2544, 2020.

390 Toomey, T., Amores, A., Marcos, M., Orfila, A., and Romero, R.: Coastal Hazards of Tropical-Like Cyclones Over the Mediterranean Sea, Journal of Geophysical Research: Oceans, 127, e2021JC017 964, https://doi.org/https://doi.org/10.1029/2021JC017964, 2022.

Torres, R. R. and Tsimplis, M. N.: Sea level extremes in the Caribbean Sea, Journal of Geophysical Research: Oceans, 119, 4714–4731, 2014.

woldometers: Caribbean Population, https://www.worldometers.info/world-population/caribbean-population, 2022.

395 Woodworth, P. L., Hunter, J. R., Marcos, M., Caldwell, P., Menéndez, M., and Haigh, I.: Towards a global higher-frequency sea level dataset, Geoscience Data Journal, 3, 50–59, 2016.

Zhang, Y. and Baptista, A. M.: SELFE: A semi-implicit Eulerian–Lagrangian finite-element model for cross-scale ocean circulation, Ocean modelling, 21, 71–96, 2008.

Zhang, Y. J., Ye, F., Stanev, E. V., and Grashorn, S.: Seamless cross-scale modeling with SCHISM, Ocean Modelling, 102, 64–81, 2016.
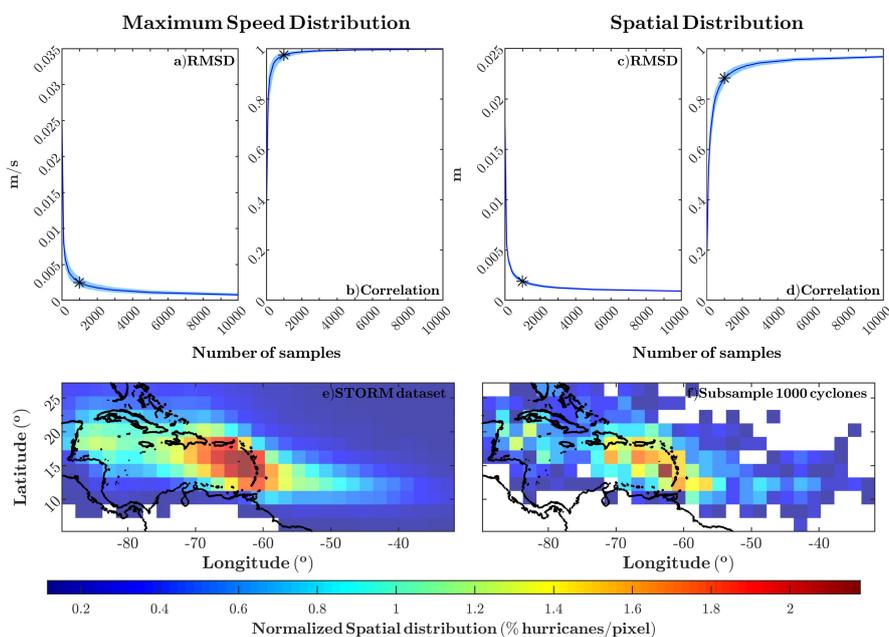
Figure 1. Statistical tests carried out on the Caribbean cyclone subsamples using as variables: the maximum speed for the panels a), b), and the spatial distribution for the panels d) and e). Where the blue line represents the median and the light blue part represents the range of values between the percentiles 95 and 5, on each panel. The panels f) and g) represents, respectively, the the percentage of cyclones per pixel for the total sample (∼ 25000 TC) and the subsample selected for the project (∼ 1000 TC), marked on the rest of the panels.
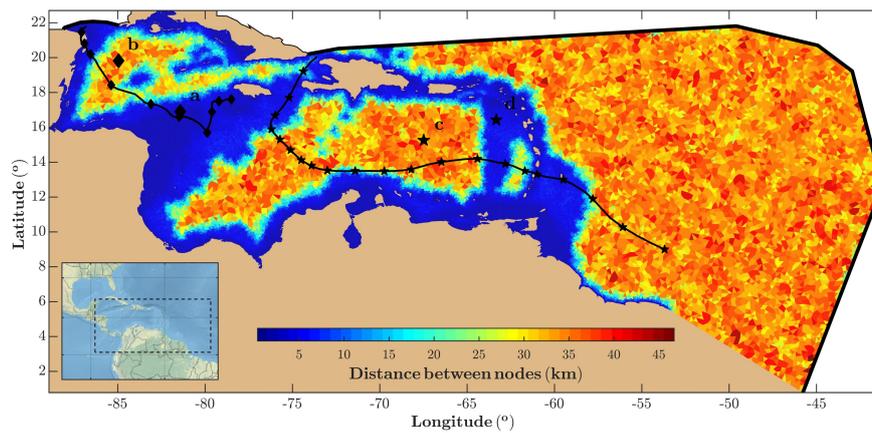
Figure 2. Map of the domain of simulation in the lower left-hand corner, and the computational grid. The colours represent the distance between nodes in the computational grid. The black lines represent the open boundaries of the model. The black lines with star and diamond markers represent the trajectory of the real hurricanes simulated for the validation, Tomas and Wilma respectively. Using the same markers the buoys used for the validation are represented, c and d for Tomas, and a, b for Wilma.
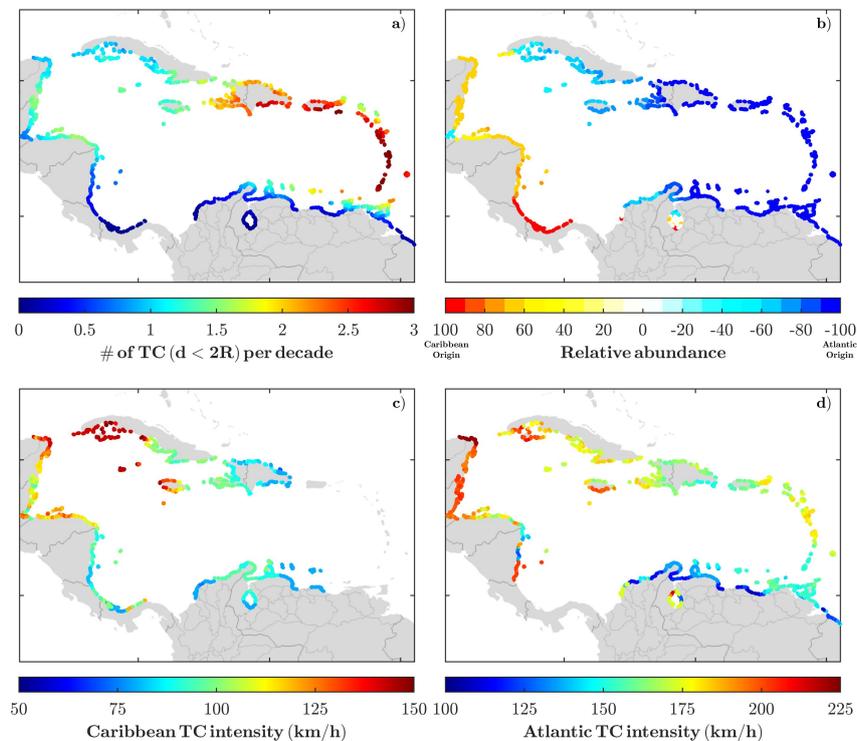
Figure 3. Characteristics of TCs affecting the Caribbean coasts. The top panel a) shows the number of hurricanes per decade affecting each coastline. That is, those that pass at a distance (d) less than twice the radius of maximum speed (R). Panel b) shows a measure corresponding to the family of TCs that most affect that area, in percentage. In this way, 0 is obtained if both families affect equally, and in colour the percentage of the one that affects more at each point. The entire red zone is dominated by hurricanes generated in the interior of the Caribbean Sea, while the blue zone is more influenced by hurricanes of Atlantic basin. Panels c and d) show the intensity of TCs in each family, those generated in the Caribbean, and those in the Atlantic respectively. We call intensity to the median maximum wind speed of each hurricane affecting that area.
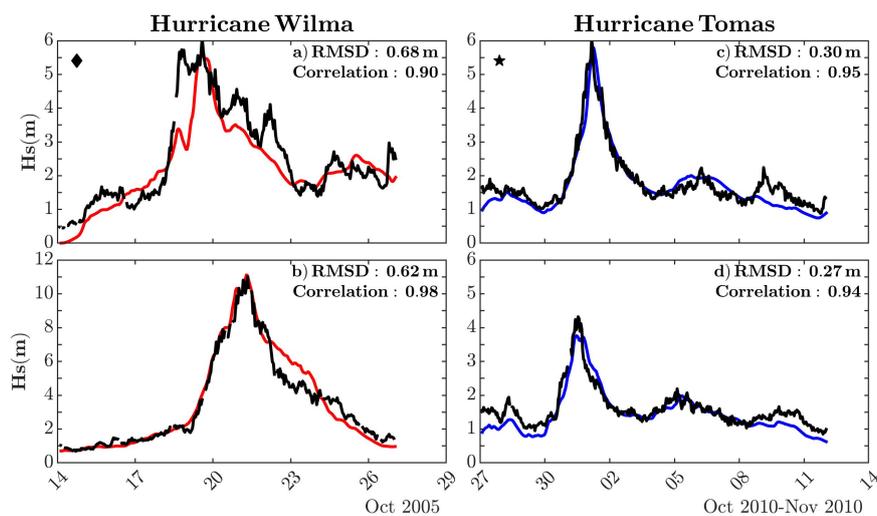
Figure 4. Comparison between modelled significant wave height (black line) and the observations from in-situ buoys for both Wilma (in red) and Tomas (in blue) hurricanes. Two buoys were simulated for each hurricane for the validation, the letter of each panel indicates which buoy it is on the map in the figure 2.
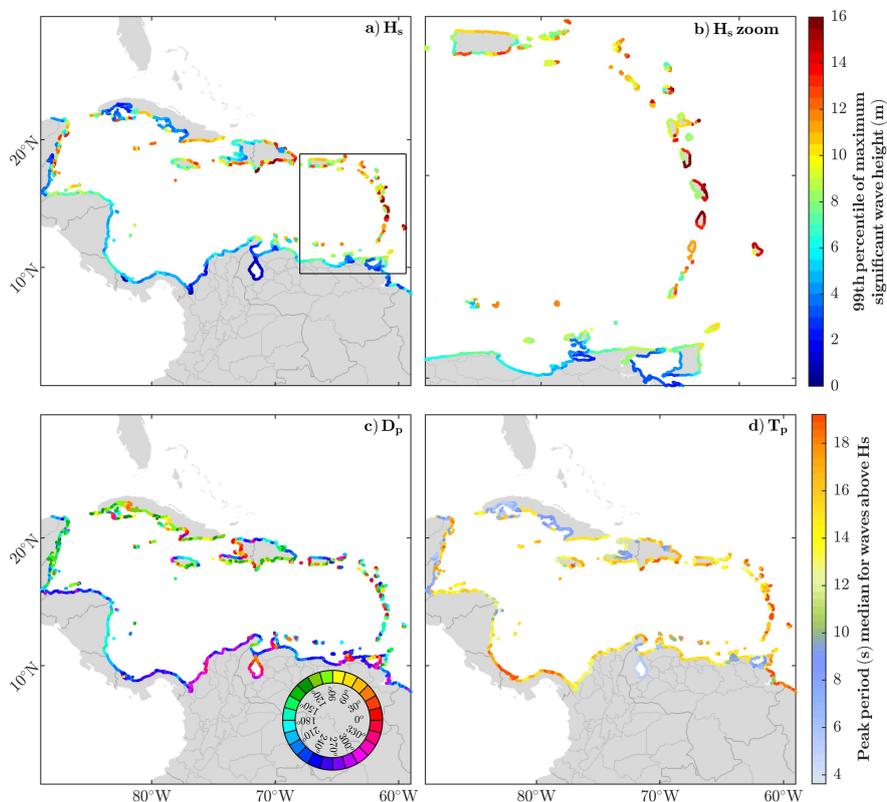
Figure 5. Fully coupled simulation results. Both panels a) and b) represents the 99_{th} percentile of the maximum H_s for each hurricane, for the whole domain (a) and a zoom on the Antilles area (b). Panels c) and d) are the median of peak period (T_p) and the direction of peak (D_p) for the highest waves respectively. All panels were calculated using the nearest point to coast at a depth of 20 m, to avoid problems with poor shore resolution.
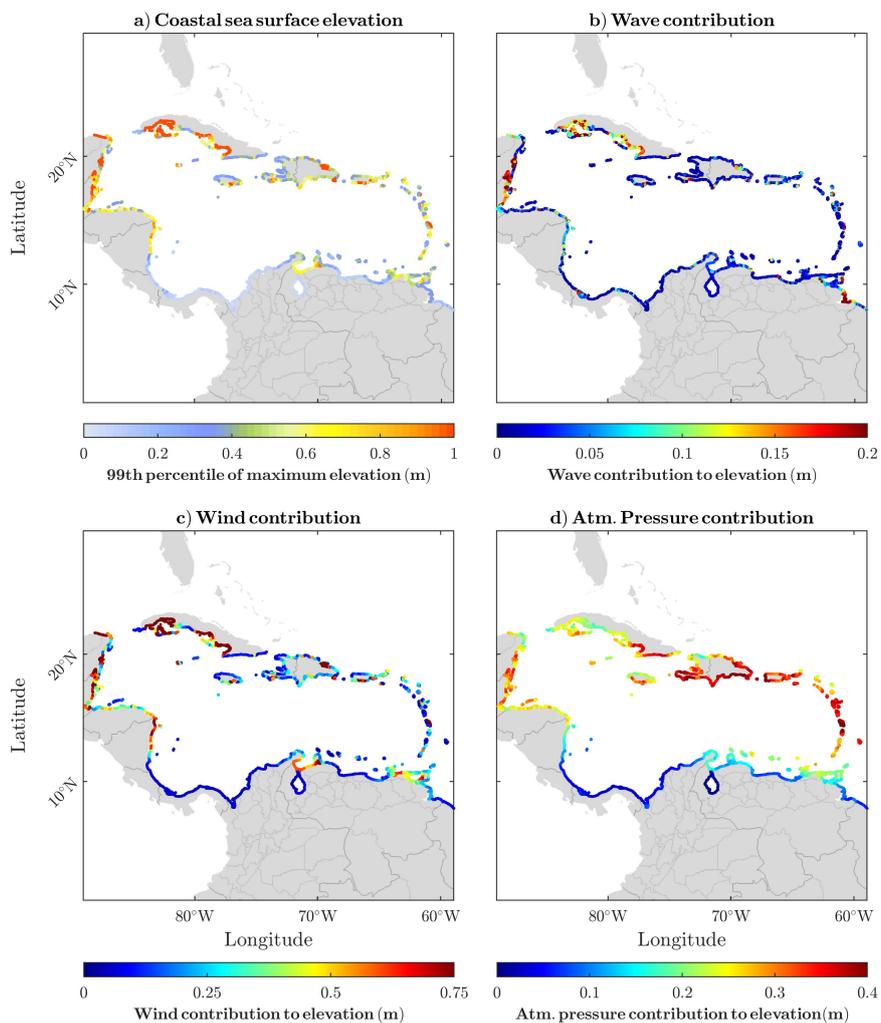
Figure 6. 99_{th} percentile of the maximum sea surface elevation for each hurricane along the Caribbean coast (a) and its contributions: wave setup (b), wind (c) and atmospheric pressure (d) in absolute terms. All panels were calculated using the nearest point to coast at a depth of 20 m, to avoid problems with poor shore resolution.
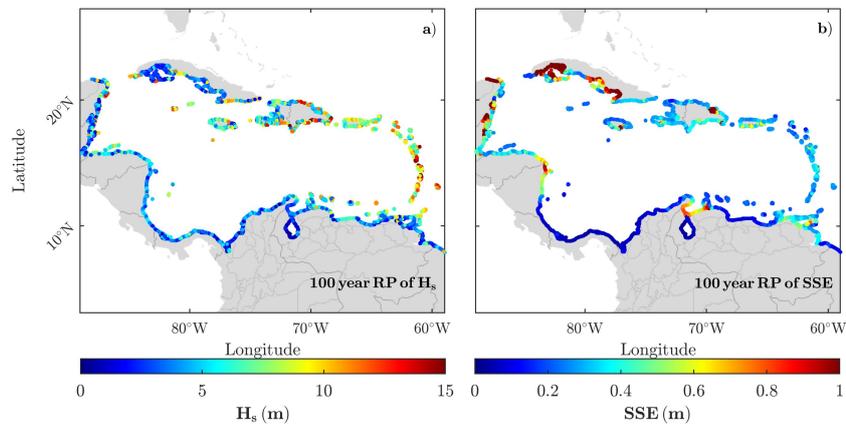
Figure 7. Return Levels of the variables H_s in panel a), and SSE panel b) for 100 years return period.